

Received December 12, 2020, accepted January 4, 2021, date of publication January 20, 2021, date of current version January 28, 2021.

Digital Object Identifier 10.1109/ACCESS.2021.3053144

# Room-Level Localization System Based on LoRa Backscatters

ANTONIO LAZARO<sup>1</sup>, (Senior Member, IEEE), MARC LAZARO, AND RAMON VILLARINO<sup>1</sup>

Department of Electronic, Electric, and Automatic Engineering, Rovira i Virgili University, 43007 Tarragona, Spain

Corresponding author: Antonio Lazaro (antonioramon.lazaro@urv.cat)

This work was supported by the Spanish Government under Project RTI2018-096019-B-C31 and Grant PRE2019-089028.

**ABSTRACT** The aim of this paper is to propose a novel room-level localization approach to locate LoRa backscatter devices, which can be easily embedded into wearable devices or smartphones. The advantages of this system lie in its series of low-cost, low-power, low-complexity and long-range features. LoRa backscattering operates by alternatively connecting an antenna, through a switch, to two loads with high reflection coefficients and opposite phase. The result is a frequency shift of the LoRa incident signal equal to the backscatter switching frequency. The localization system comprises several LoRa receivers distributed among the rooms, a LoRa transmitter located at a central point and the backscatter device, which is carried or worn by a subject. The position of the LoRa backscatter device can be determined by comparing the received signal strength between all receivers. In order to improve the accuracy of the system, different machine learning classifiers were compared. System performance was tested in a real-life scenario, achieving an accuracy up to 89.7% using linear discriminant analysis (LDA).

**INDEX TERMS** Backscatter communications, LoRa, localization, wireless sensor networks, RFID, zero-power sensor, Internet of Things (IoT).

## I. INTRODUCTION

Modulated backscatter communication systems are based on a device that reflects received radiofrequency (RF) signals from an RF transmitter and introduces a modulation that is used to transmit data. The use of modulated backscatter communications has expanded rapidly since they were first introduced by Stockman in 1948 [1]. This technology is the basis for radiofrequency identification (RFID) [2]. Recently, several low-power communication systems based on backscattering communications have been investigated [3]–[6]. In spite of these efforts, low-power wireless systems based on backscattering communications are not widely used. Traditional backscatter communications operate passively, meaning that the RF source has to be positioned near the backscatter device. However, ambient backscatter communication systems have recently emerged as a technology with great potential for future low-power communications for the internet of things (IoT) [4], [7]. These systems propose using surrounding signals (e.g. FM and TV towers, mobile signals, and Wi-Fi access points) as RF sources for backscatter devices.

The associate editor coordinating the review of this manuscript and approving it for publication was Alessandro Pozzebon.

One of the main challenges in the implementation of a large area wireless sensor network is the deployment and maintenance cost. To this end, low-power wide-area networks (LPWANs) such as UNB (ultra-narrow band), LoRa, and SigFox have become popular for machine-to-machine (M2M) IoT applications [8], [9]. LoRa is based on a robust chirp spread spectrum (CSS) technique operating at industrial, scientific and medical (ISM) bands (433 MHz, 868 MHz, and 915 MHz) [10], [11]. Although LoRa was originally designed for long-range outdoor communications, the high sensitivity of the LoRa receiver [12] and the low attenuation of the walls at these frequencies make LoRa an interesting option for indoor coverage [13], [14]. Lately, LoRa-based modulation was used for backscatter communication environments and achieved long-range operation [15]–[18]. In a previous work [19], we presented a LoRa backscatter communication system for monitoring deeply implanted medical devices.

In recent years, indoor localization systems have generated great interest due to their potential applications [20]–[22]. Most of the methods proposed in the literature as well as commercial systems focus on improving localization precision [23]. In some applications, such as autonomous robot guidance [24], localization accuracy is fundamental because

they require an exact location in a coordinate system. Performance depends greatly on the method used (time of arrival (ToA), time difference of arrival (TDoA), angle of arrival (AoA), or received signal strength indicator (RSSI) based), the environment, the attenuation introduced by objects, movement, and the localization algorithm employed. Depending on the localization method, different wireless systems have been explored: Wi-Fi, Bluetooth, UWB, modulated continuous wave (FMCW) radar, RFID, etc. LoRa-based localization systems have recently been proposed for indoor and outdoor environments [25]–[28]. Some of these systems were compared in [1], [2]. Their precision often increases with the number of anchors [29], [30] and these systems require LOS (line of sight) scenarios [31].

Another interesting group of localization techniques includes those that are based on fingerprint classification. In this case, the system estimates the location of an object by matching received signal strength indicator (RSSI) measurements with the closest location fingerprints. The RSSI measurements are often obtained from Wi-Fi access points [32] or Bluetooth beacons [33], [34] in indoor applications or Sigfox, LoRaWAN [35] or mobile communications in large areas [36]. However, these methods require a calibration of the system by recording the exact location on a map. Two main groups of techniques have been reported for classification in these systems: neuronal networks [37], [38] and machine learning techniques [39]. The main drawback of previous localization methods is that the high number of anchors and the manual calibration procedure decrease the system's return on investment (ROI). However, there are other applications in which knowing an approximate area, such as a room [34], [40], [41], is sufficient. Within the various medical applications, monitoring activities of daily living (ADL) [42]–[45] constitute an example of the second group. A major challenge for these applications is that the tracking devices must be noninvasive and private because they are intended to be used by the elderly. Therefore, the devices must be worn and the battery lifetime must be very long to avoid continuous recharges that can cause the user to stop using the system. Both the installation of the localization system and the cost mean that a reduced number of anchors capable of covering large areas (e.g. care facilities or hospitals) have to be installed. From a practical perspective, it should be noted that in most indoor localization methods, when the number of anchors used is small (or when the cost of installing several anchors is prohibitive), the precision is around several meters [33]. In other words, they can be used to roughly recognize a room.

This paper describes the study of the performance and viability of an indoor room-level localization system based on LoRa signal backscattering. This work aims to contribute to the improvement of human and social welfare through the application of the system in fields such as patient management in hospitals and care facilities, capacity monitoring in establishments of different types, autonomous buildings, etc. Compared to other systems based on active beacons

(e.g. Bluetooth, Wi-Fi, or UWB), LoRa backscatter stands out for its lower power consumption and long range due to the high sensitivity of LoRa receivers. This LoRa backscatter device can be embedded in a wrist band or any other wearable device, thereby obviating the need for uncomfortable, heavy electronics. The localization system is made up of several LoRa receivers distributed in the different rooms, a LoRa transmitter located at a central point, and the backscatter device, which is carried or worn by an individual. Commercial low-cost LoRa modules were used in the experiments to validate the system. A simple algorithm based on the reception of the highest signal strength was used to determine the position (the room where the user is). In order to improve accuracy, we compared different machine learning algorithms. In these cases, algorithm training was accomplished by acquiring a set of samples while the user moves randomly within each of the rooms. The random point acquisition greatly accelerates the training procedure. It is only necessary to know which room the samples were taken in, and not the coordinates of the receivers or the transmitter. Parameters such as transmitter power and propagation model are also not necessary to program the algorithms. This simplifies the training procedure and practical implementation in real environments.

This paper is organized as follows. Section II describes the system, including the proof of concept prototype for the LoRa backscatter. A propagation model is proposed to check the algorithm based on simulated data. The simulated results are described in Section III. Our experimental results are presented in section IV. Section V compares the features of the proposed room-level localization technique with other localization technologies. Finally, section VI summarizes our conclusions.

## II. SYSTEM ARCHITECTURE OVERVIEW

This paper proposes the use of a backscatter device that reflects the data signal from a LoRa transmitter but with the frequency shifted to a different LoRa channel. A set of LoRa receivers tuned to this shifted channel receives the data packets and measures the received signal strength indicator (RSSI) and signal-to-noise ratio (SNR) for each one. The LoRa receivers are placed in different rooms, so each room can be identified by comparing the RSSI collected by the receivers. The receiver with the highest RSSI level will determine the location of the backscatter. Advanced fingerprint algorithms can be employed to improve the decision. A diagram of a possible scenario is shown in Fig. 1. The LoRa backscatter system can be easily miniaturized, so it can be worn on the wrist (see Fig. 2). Furthermore, it stands out for its low power consumption compared to other beacons because it does not have to generate RF signals or process the incoming LoRa packets. An important consideration is that the power of the backscattered signal is significantly reduced due to the two-way propagation, but this drawback is compensated by the high sensitivity of the LoRa modulation which, compared with other modulations, is capable of demodulating signals of

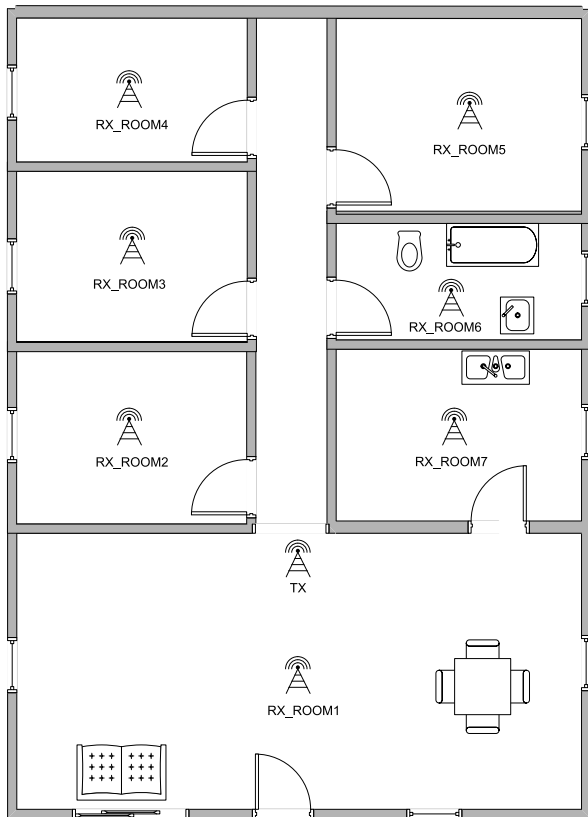


FIGURE 1. Example of typical Tx and Rx placement in a house.

up to 20 dB under the noise floor [6]. LoRa receivers exhibit an impressive sensitivity down to  $-148$  dBm depending on the spread factor employed (Semtech SX1276 [6]).

We used low cost LoRa transceivers (ESP32 TTGO with Semtech SX1276) in our experiments. Each of them has a built-in ESP32 microcontroller from Espressif, with a Wi-Fi and Bluetooth connection, and a Semtech SX1276 LoRa module set at the 868 MHz ISM band with a default transmission power of 17 dBm. Semtech SX1276 allows the user to configure, among many others LoRa and radio parameters, the transmission power from 2 dBm up to 20 dBm. The cost of this LoRa transceiver is less than \$10 and no hardware modification is needed. A Wi-Fi link is used to send the data to a cloud database. Alternatively, the data can be transmitted to the LoRa transmitter by a conventional LoRa link, which works as a gateway to upload the data to a cloud database. This second method can be used in industrial environments or in buildings without coverage in some areas or without any coverage at all. Data are transferred to the cloud by means of the MQTT (Message Queue Telemetry Transport) protocol. Each receiver publishes the RSSI and SNR measurements in a MQTT topic. To avoid errors arising from lost packets or uploading delays, the transceiver sends each packet with an identifier, which might be just a counter. This makes it possible to synchronize receivers. Upon reception, the receivers publish a message to the MQTT broker with the packet identifier, the room identifier, and the measured RSSI and SNR.

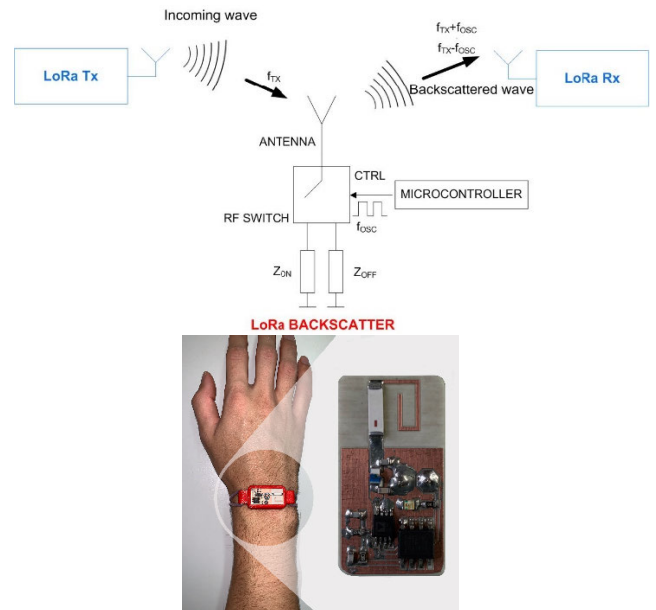


FIGURE 2. Block diagram of the backscattering system (top) and photograph of a prototype (bottom).

#### A. BACKSCATTER PROTOTYPE

A block diagram of the backscatter is shown in Fig. 2. The backscatter consists of an antenna connected to an RF switch that loads the antenna and switches between two states with a high reflection coefficient (e.g. open and short circuit). The antenna is tuned to the ISM band (865–869 MHz). In a proof of concept prototype, we used the ADG902 CMOS switch from Analog Devices and the low-power microcontroller ATtiny402 from Atmel. The square-wave oscillator controls the switch at the oscillation frequency  $f_{osc}$  and is implemented with the microcontroller. The waveform is generated using the pulse-width modulation (PWM) output of the microcontroller. The Semtech SX1276 LoRa transceiver, which can work from 137 MHz to 1020 MHz, was used in these experiments. This made it possible to cover European, North American, and Asian ISM bands. Due to the high tolerance to frequency deviations of this module, the Semtech transceiver is capable of demodulating packets, despite the possible oscillator drifts during the backscatter communication. Even in the rare case of not being able to demodulate the data due to a considerable frequency shift, the SX1276 has an automatic frequency correction functionality (AFC) to readjust the reception frequency. The low-power microcontroller (ATtiny402) was used as a proof of concept prototype to generate the data identification and connect to potential sensors.

The total current consumption when the microcontroller wakes up, working at a 1 MHz clock speed with an operating voltage of 3.3 V, is  $890 \mu\text{A}$ . The power consumption of the switch, at less than  $1 \mu\text{A}$ , is negligible. This total value is considerably lower than that of Bluetooth LE modules that typically require 7 to 15 mA when they are in the reception or transmission states. One interesting aspect to mention is

that the backscatterer device has no transmission or reception mode, since it is not capable of processing or generating RF signals. Therefore, the backscatterer device just bounces or stops reflecting the LoRa signal.

The analysis of the modulated backscatter can be found in [46]. The backscattered power is proportional to the differential radar cross-section  $RCS_{dif}$  [47]:

$$RCS_{dif} = \frac{\lambda^2}{4\pi} G_{tag}^2 |\Gamma_{ON} - \Gamma_{OFF}|^2 m \quad (1)$$

where  $\lambda$  is the wavelength,  $G_{tag}$  is the backscatter antenna gain, and  $m$  is the modulating factor, which, assuming an ideal 50% duty cycle, will have a value of  $1/\pi^2$ .  $\Gamma$  is the power reflection coefficient given by [47]:

$$\Gamma = \frac{Z_L - Z_a^*}{Z_L + Z_a} \quad (2)$$

where  $Z_L$  and  $Z_a$  are the load impedance for each state (ON or OFF) and the antenna impedance, respectively. A high reflection coefficient with a difference of  $180^\circ$  is needed to maximize the backscattered power. This situation can occur if the antenna resonates in the band ( $\text{Im } Z_a = 0$ ) and each of the two impedance states is out of phase (e.g. close to short circuit and open circuit). Fig. 3 shows the measured reflecting coefficients at the antenna port for the two switch states. The modulation gain relative to the ideal backscatter  $|\Gamma_{ON} - \Gamma_{OFF}|^2/4$  is 0.62 at 868 MHz (or  $-2$  dB).

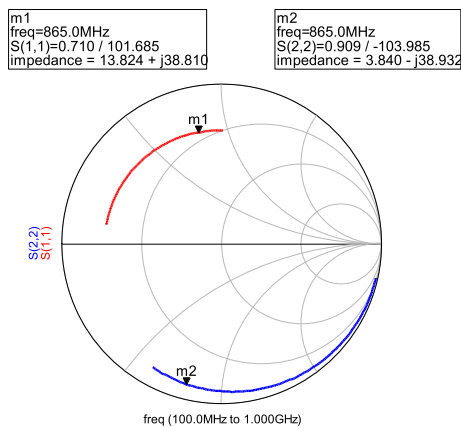


**FIGURE 3.** Measured reflection coefficients of the ADG902 switch ( $S_{11}$  state OFF,  $S_{22}$  state ON) as a function of the frequency between 100 – 1000 MHz.

Figure 4 shows a screenshot of the measured spectrogram using a software-defined radio (SDR) receiver (RTL-SDR dongle). In this measurement, the RTL-SDR was used as a low-cost spectrum analyzer. The spectrogram is obtained from the phase and quadrature (IQ) samples measured by the SDR module. Both the transmitted LoRa channel and the shifted signal to  $f_{TX} \pm f_{osc}$  can be seen when the backscatterer is enabled. In this example, a spread factor ( $SF$ ) of 12, a bandwidth ( $BW$ ) of 125 KHz, and a backscatter oscillation frequency ( $f_{osc}$ ) of 300 kHz was employed. Therefore, a LoRa receiver tuned to this shifted channel can detect the presence

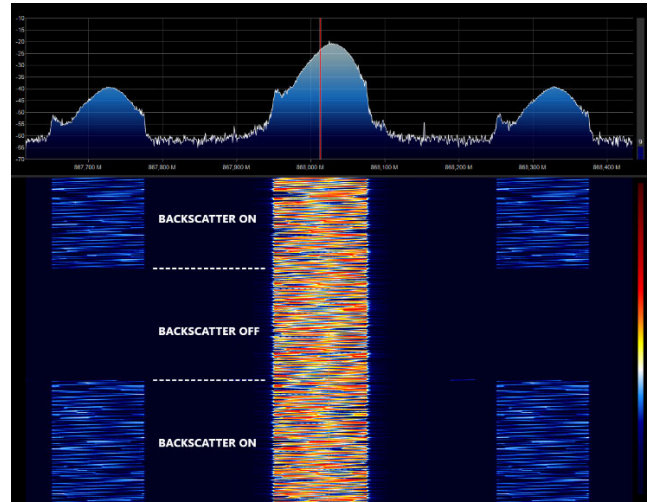


**FIGURE 4.** Spectrogram of a transmitted channel and backscatter signals when the backscatter is enabled and disabled.

of the backscatter and demodulate the packets as long as the backscatter modulator is on.

## B. PROPAGATION MODEL

The method proposed is based on the measurement of the RSSI from different receivers tuned to the frequency channel shifted by the backscatter. In this section, we propose an empirical model to perform simulations of coverage area and localization rates.

The received power ( $P_R$ ) can be expressed as in an RFID system using the radar equation [47]:

$$P_R = \frac{P_T G_T}{4\pi d_T^2} RCS_{dif} \frac{1}{4\pi d_R^2} \frac{\lambda^2}{4\pi} G_R \quad (3)$$

where  $P_T$  is the transmitted power,  $G_T$  the transmitter antenna gain,  $G_R$  is the receiver antenna gain,  $RCS_{dif}$  is the differential radar cross-section of the backscatter, and  $d_T$  and  $d_R$  are the distance from the transmitter to the backscatter and from the backscatter to the receiver, respectively. The receiver power increases when the backscatter is close to the transmitter or the receiver. The locus of points with constant received power approximately describe an ellipse.

However, the Friis model (3) is only valid in free space or in situations where the antennas have high directivity, which avoids multipath interference. In order to include multipath propagation, an empirical model is often considered. The RSSI is the received power expressed in dBm [19]:

$$P_R (dBm) (d_T, d_R) = P_R (dBm) (d_0, d_0) - 10n_1 \log \left( \frac{d_T}{d_0} \right) - 10n_2 \log \left( \frac{d_R}{d_0} \right) - L_{wall} + X \quad (4)$$

Eqn. (4) is split into two parts considering the two existing propagation paths: transmitting to the backscatter and backscattering to the receiver. In (4),  $d_0$  is the reference distance (i.e. the midpoint between transmitter and receiver

$d_0 = (d_{Tx-Rx}/2)$ ,  $P_R(d_0, d_0)$  is the average received power at  $d_0$ ,  $n_1$  and  $n_2$  are the path loss exponents, whose values depend on the environment and the height of the antennas. Typical values for indoor environments vary between 2.5 and 3.  $L_{wall}$  are the losses due to the diffraction and attenuation of the walls and  $X$  is a random variable that takes into account the attenuation due to multipath propagation.  $P_R(d_0, d_0)$  can be found experimentally from the regression of measured data.  $P_R(d_0, d_0)$  is a function of the transmitted power and the gain of the antennas. However, it is also a function of the height of the antennas and depends on the diffraction. However, in this section, to perform our simulations, we consider the following expression derived from the Friis transmission equation.

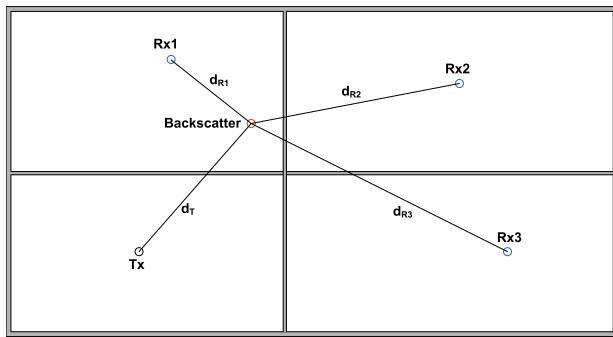


FIGURE 5. Diagram used for the description of the propagation analysis.

A typical deployment scenario is shown in the diagram in Figure 5. The attenuation due to path loss between the transmitter and backscatterer is equal from all the receivers, but the power of the received signals depends on the distance between each receiver and the backscatterer  $d_{Ri}$  and the number of walls that each signal goes through. It is expected that the maximum received power will be that of the receiver that is in the same room as the backscatterer because it will be closer to it and attenuation due to the walls will not be an issue.

Typical wall attenuation at 900 MHz for a brick wall is 5 dB and 15–18 dB for a double reinforced concrete wall [48]. In the model, the distribution presented by the random variable  $X$  can be considered of the log-normal type  $X(\text{dB}) \sim N(0, \sigma)$ , where  $\sigma$  [dB] is the standard deviation and experimental results yield values between 2 and 4 dB for a single path [49] (in this case a double path due to the backscatterer channel is expected).

The coverage probability ( $Prob$ ) is that in which the average received power or RSSI,  $P_R$  (dBm), is higher than the receiver sensitivity  $S$  (in dBm). For a log-normal distributed channel this is given by [50]:

$$Prob(P_R > S) = \frac{1}{2} \operatorname{erfc} \left( \frac{S - P_R}{\sqrt{2}\sigma} \right) \quad (5)$$

where  $\operatorname{erfc}$  is the complementary Gauss error function. For a  $\sigma = 8$  dB and a received power of 10 dB above the sensitivity (fading margin), the coverage probability is about 90%.

LoRa receiver sensitivity depends too on the noise figure of the receiver and the bandwidth ( $BW$ ). It is computed from the noise floor plus the required signal to noise ratio (SNR) [12]:

$$S \text{ (dBm)} = -174 + 10 \log(BW) NF(\text{dB}) + SNR(\text{dB}) \quad (6)$$

where  $BW$  is the bandwidth of the LoRa signal and  $NF$  is the LoRa receiver noise figure. The SNR is negative and can be approximated by a function of the spreading factor (SF), which can be selected in LoRa transceivers from 7 to 12 [12]:

$$SNR \text{ (dB)} = -7.5 - 2.5(SF - 7) \quad (7)$$

One of the reasons why the LoRa transceiver is used in this system is its high sensitivity, which allows the detection of the backscatter in indoor environments in spite of the attenuation typically experienced in such spaces. From (6), for a spread factor of 12, a bandwidth of 125 kHz, and assuming a typical noise figure of 6 dB, the receiver sensitivity is  $-137$  dBm.

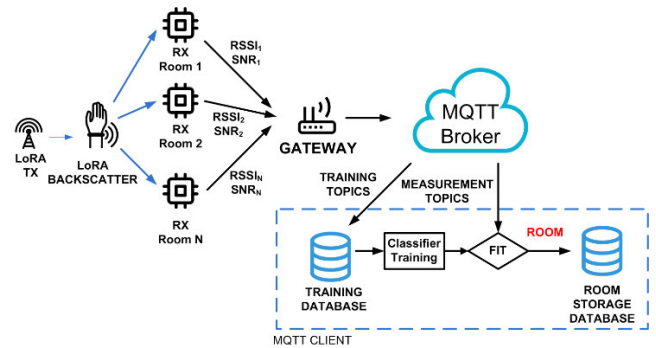


FIGURE 6. Block diagram of the classification procedure.

### C. ROOM-LEVEL CLASSIFICATION

The classification process is schematically described in Fig. 6. The LoRa transmitter regularly transmits packets using a counter for packet identification. The transmission time interval (packets transmitted per second) can be configured depending on the desired tracking frequency or application. When it strikes the device, the signal coming from the LoRa transmitter is backscattered towards the receivers located in each room to identify the signal. Each receiver has been tuned to the shifted frequency channel. The received RSSI and SNR measured by the LoRa transceiver and the packet identification number are sent to the MQTT broker. In this case, a Wi-Fi transmission was used because the ESP32 has a built-in Wi-Fi transceiver. However, in the absence of Wi-Fi coverage, the receiving node can be configured to transfer the message via LoRa to a gateway with an internet connection, which will upload the data to the MQTT broker. A custom Mosquitto broker was used in the experiment but other MQTT brokers can also be used. There are two modes of operation: training mode and the normal operation mode. In the former, the data are stored in a database for later use in the training of the classifiers. Then, to train the system, data are provided together with

the room where the backscatter is, allowing the system to learn the footprint of each backscatter location. To indicate the room where the backscatter is located during the training stage, a message is sent to an MQTT configuration topic using a mobile app. After that, the training data collected are used for training the machine learning model. The MQTT client is implemented in Python using the Eclipse MQTT Paho module. The scikit-learn module was used for machine learning. In the normal operation mode, the room number is determined by the measured RSSI and SNR data, which are obtained from the subscription to the respective MQTT topics of the receivers. If any of the receivers do not receive the backscattered packet because they are outside its coverage area, the minimum value of RSSI (sensitivity) and SNR will be assigned. The simplest classification method consists of assigning the room to the index of the receiver with the highest SNR or RSSI. As the resolution in the RSSI measurement is only 1 dBm for the LoRa transceiver used in this work, the use of the SNR measurements seems to be the most appropriate option due to their higher resolution, which tends to yield better results. In any case, the room can be determined with both the RSSI and the SNR measurements, providing the system a double-check calculation. If advanced machine learning algorithms are used for the room classification, the room index is obtained by running the trained classifier. The simulated and experimental results with different classifiers will be described in the coming sections.

### III. SIMULATIONS

Figure 7 shows the received power in dBm computed using the model (3)-(4) as a function of the backscatter location at 868 MHz. We considered a 50 m distance between transmitter and receiver. Fig. 7a shows the ideal free space case, whereas Fig. 7b shows a scenario with decay factors ( $n_1$  and  $n_2$ ) of 2.5. The EIRP transmitter power was 20 dBm, and the receiver antenna gain was 2.2 dBi. The gain of the backscatter antenna was  $-1$  dBi (the typical surface-mount antenna gain). In the simulations, the measured backscatter gain and the ideal square wave waveform were used. An indoor scenario resulted in a considerable reduction in receiver power. However, these simulation results show that a LoRa backscatter can be detected within an area of about  $100 \text{ m}^2$ , although the attenuation of walls or other objects would decrease this coverage area. We present measured results in a house in the next section.

A series of simulations were performed to validate the proposed method. Six rooms of different sizes covering an area of  $40 \text{ m} \times 40 \text{ m}$  were considered. The received power obtained from the model (4) are shown in Fig. 8. A value of 10 dB was taken for wall attenuation with a standard deviation of 8 dB. The transmitter was located approximately in the center of room one.

Several classifiers can be used to determine the room number associated with the RSSI measured at each one of the receivers. The simplest method consists of determining the

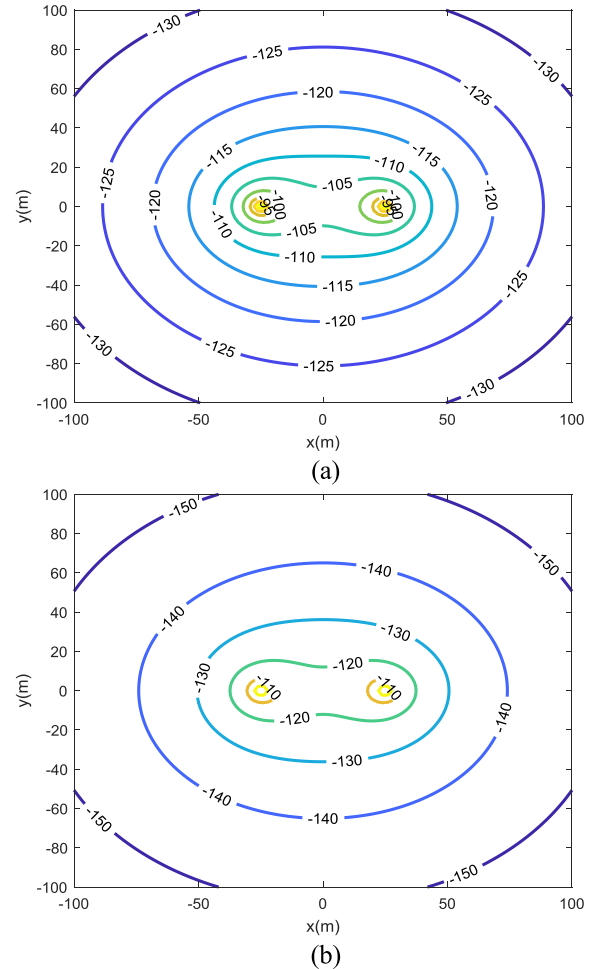


**FIGURE 7.** Contour map of the received power as a function of the backscatter location (a) in free space and (b) considering a propagation decay factor of 2.5.

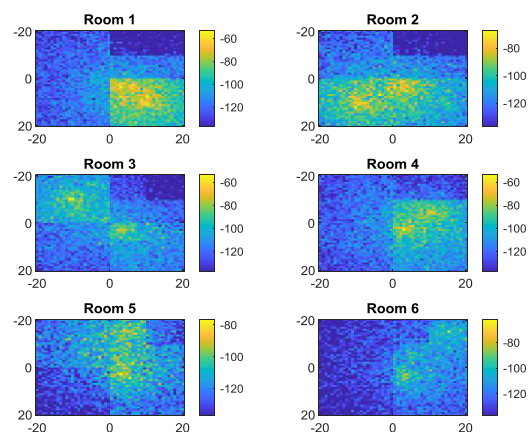


**FIGURE 8.** Contour map of the received power as a function of backscatter location for each receiver location.

room number through the receiver with the best power reception. Fig. 9 shows the classified rooms for the last simulated scenario using the simplest RSSI classifier, where the room is assigned to the receiver that collects the strongest RSSI

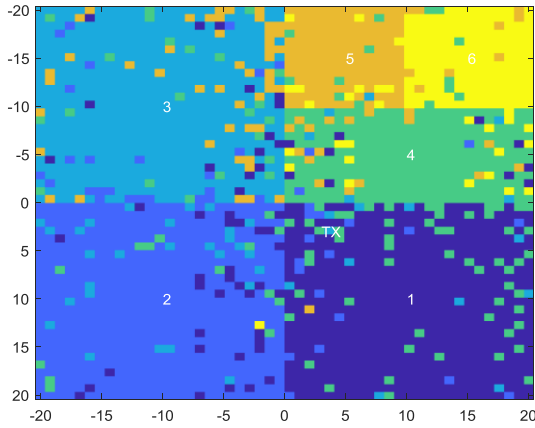


**FIGURE 9.** Color map that shows the classified room using an RSSI level classifier. Each room is represented by a different color. The position of the receiver is indicated with the room number. The position of the transmitter is also shown.

**TABLE 1.** Accuracy (%) as a function of classifier.

Room	HRL	LR	LDA	KNN	CART	NB
1	84	93	94	90	88	90
2	87	91	91	94	89	90
3	85	96	97	93	91	93
4	80	80	90	80	77	82
5	85	72	83	90	79	83
6	92	54	94	89	97	94
Average	85.6	89.3	92.5	91.5	87.0	89.3

Method: HRL: Highest RSSI level; LR: Logistic regression; LDA: Linear discriminant analysis; KNN: Neighbors classifier; CART: Decision tree classifier; NB: Gaussian naïve Bayes

signal. This method has the advantage of not requiring a training step. Although this method worked reasonably well in the presence of noise, other classifiers were also analyzed. Classifiers implemented in Python scikit-learn machine learning module [51] were used for comparison. The classifiers were trained with 20% of the samples (simulated reception powers for several backscatter locations). The samples were chosen at random and the other 80% were used to test the trained classifier. Table 1 compares the accuracy obtained for each classifier. The best classifier found was linear discriminant analysis (LDA), which achieved an accuracy of up to 91.5%.

Table 2 shows the confusion matrix  $C$  for the linear discriminant analysis (LDA) classifier. Each element of this matrix  $C_{ij}$  is equal to the number of observations known to be in the room  $i$  and predicted to be in the room  $j$ . For example, in the first row, the first column indicates the room where the backscatter is, in this case room one. The algorithm was correct in its predictions in 93.84% of cases, but in 3.07% of cases, it determined that the backscatter was in room two, in 1.54% it predicted room three and in 1.54% room four. The results shown in Table 2 have been normalized by the

**TABLE 2.** Normalized confusion matrix in % using linear discriminant analysis (LDA).

Room	1	2	3	4	5	6
1	93.84	3.07	1.54	1.54		
2	3.91	91.40	4.69			
3		0.85	96.58	2.56		
4	4.92		3.27	90.16		1.64
5			6.89	3.45	82.75	6.89
6					5.71	94.28

total number of samples. Note that to improve readability the values equal to zero have been left blank. As the table shows, there was a small degree of confusion with neighboring rooms.

#### IV. EXPERIMENTAL RESULTS

The proposed room-level localization system was tested in a complex scenario like a house. Several experiments were conducted to determine the coverage of the LoRa backscattering system. Fig. 10 shows a heatmap of the received RSSI for the different rooms equipped with receivers. The backscatter was placed on the wrist of a volunteer moving along different points on a grid that was used to plot the heatmap. The transmitter was located approximately in the center of the house (in the hallway) and a receiver was located in another room separated by walls. The receiving power strength on the receiver increased when the backscatter was near the transmitter or receiver. But reasonable coverage (exceeding  $-122$  dBm) was achieved in all situations. In addition, the backscatter signal could also be received by the nearest receivers. In this test, the transmitted channel frequency was 868 MHz and the receiver was tuned to the shifted channels spaced at 300 kHz. The bandwidth was 125 kHz and the spread factor was 12.

**TABLE 3.** Accuracy (%) as a function of classifier.

Room	HSL	LR	LDA	KNN	CART	SVM
1	82	82	93	90	82	88
2	89	86	83	81	81	88
3	40	97	97	98	93	93
4	56	86	86	82	82	84
Average	66.7	87.7	89.7	87.7	84.5	88.2

Method: HSL: Highest SNR level; LR: Logistic regression; LDA: Linear discriminant analysis; KNN: Neighbors classifier; CART: Decision tree classifier; SVM: Supported vector machine

The system was applied to the scenario shown in Fig. 10, where the transmitter was located in the center of the hall and four receivers were installed in the adjacent rooms. The training procedure was performed as described in section II. A comparison of the accuracy achieved in each room is summarized in Table 3. Considering the method based on the

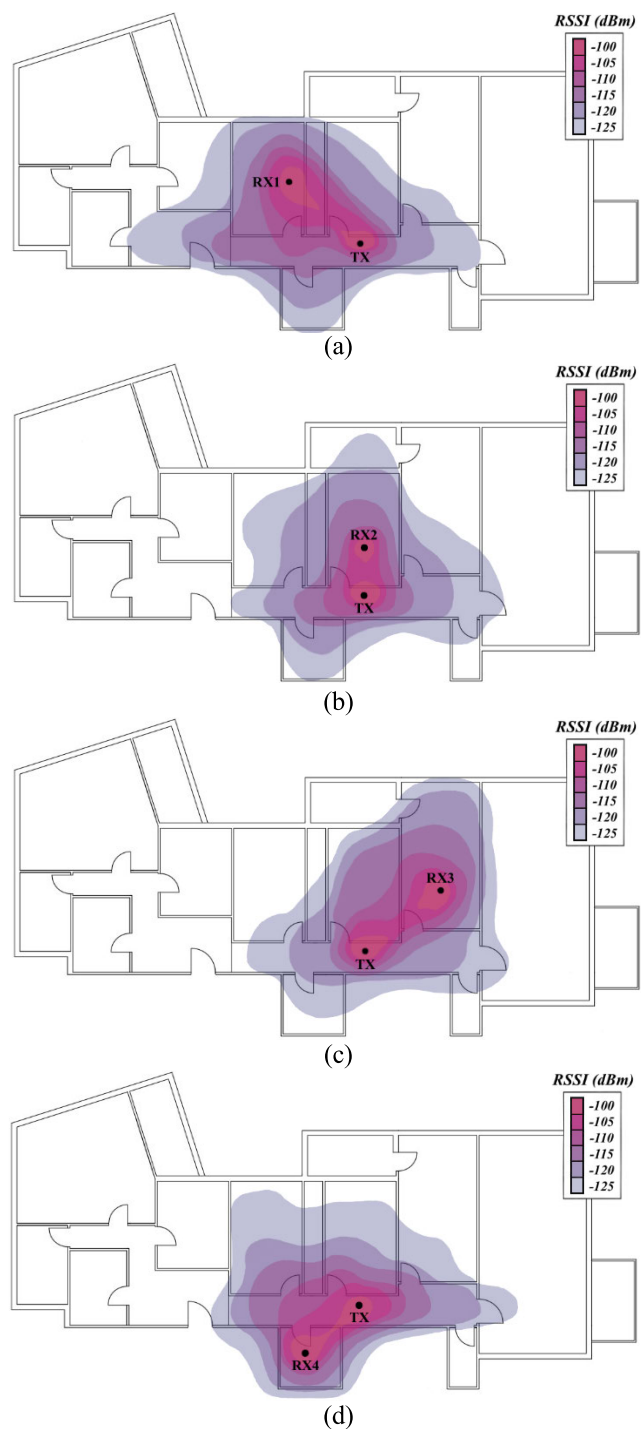


**FIGURE 10.** Measured heatmap of the received power as a function of the backscatter location for: (a) receiver RX1 located in room number one (b) receiver RX2 located in room number two, (c) receiver RX3 located in room number three and (d) receiver RX4 located in room number four (d).

highest SNR level, the degree of accuracy was very good for rooms one and two because the received strength levels were high, whereas in rooms three and four, except for some points, the degree of coverage was much lower, or even non-existent. Applying the same analysis, the accuracy for rooms three and four was worse compared to rooms one and two. This explains

**TABLE 4.** Normalized confusion matrix in % using linear discriminant analysis (LDA).

Room	1	2	3	4
1	92.5	5.0	0.0	2.5
2	7.1	83.3	4.7	4.7
3	0.0	1.7	96.6	1.7
4	10.0	4.0	0.0	86.0

the low degree of accuracy for these rooms using the simplest method. However, the other classifiers were able to achieve high degrees of accuracy in all four rooms, regardless of the room’s potential coverage. Our experimental results showed that the best average accuracy was obtained with the LDA classifier although the accuracy for room two was worse than that obtained with the other classifiers. In any case, the differences in the average accuracy among classifiers were slight, excluding the highest SNR level classifier. The Gaussian Naïve Bayes classifier (NB) was not analyzed because the measured data in the rooms did not meet the gaussianity conditions for the method that would allow it to be applied. The normalized confusion matrix for the KNN classifier is shown as an example in Table 4. The elements of the principal diagonal that present the highest percentages correspond, as expected, to the neighboring rooms. There were a significant number of cases (10%) that increased the confusion in the classification process between rooms four and one. This is because the coverage area of Rx1 and Rx4 partially overlapped with similar received levels.

## V. DISCUSSION

This section examines existing indoor localization technologies described in the literature. Although several surveys (e.g [20], [52]) on localization are available, this section aims to compare the advantages and limitations of the system proposed here in relation to other similar systems. Table 5 summarizes some of the properties, advantages and disadvantages of the technologies studied. The different technologies analyzed are described below.

### A. WI-FI

Wi-Fi networks (based on IEEE 802.1 standards) operate on ISM bands and are used to provide internet access to computers and smartphones, especially in indoor environments. Therefore, Wi-Fi is an ideal system for indoor localization and has been widely examined in the literature. Existing access points deployed for communication can be used as reference (anchor) nodes for localization without the need for additional infrastructure. However, it is sometimes necessary to install more anchors to improve accuracy, which increases the cost. Localization techniques based on RSSI measurements are the most common [53], [54]. However other techniques use the measurement of channel state information

TABLE 5. Summary of different technologies for indoor localization.

Technology	Coverage	Power Consumption	Accuracy	Cost	Method	Advantages	Disadvantages
UWB	30 m	Moderate	cm-m	High	ToA Fingerprint	Immunity to interferences	Requires special hardware on different user devices
Bluetooth	10-20 m	Low	m	Low	RSSI iBeacon	Widely available. Integrated in smartphones and smartwatches.	Sensitive to multipath
Wi-Fi	50 m	High	dm-m	Low	RSSI CSI AoA Fingerprint	Widely available	Sensitive to multipath and requires complex processing algorithms
Zigbee	100 m	Moderate	m	Moderate	RSSI Fingerprint	Easy deployment	Sensitive to multipath. Not available in smartphones
Active RFID	20 m (indoor)	Low	< 1 m	Moderate	RSSI Fingerprint	Long life battery	Expensive readers, property tags
Passive RFID	cm to few meters	Very Low	< 1 m	Low	RSSI Fingerprint	Low cost of the tags. No batteries.	UHF readers are expensive. Short range for HF systems. Environmental noise.
Ultrasound	Couple of meters	Low-Moderate	1.5-10 cm	Low	ToA	Widely used for distance measurements.	Dependence of sound velocity on temperature and humidity. Affected by ambient noise.
Acoustic	Couple of meters	Low-Moderate	cm	Moderate	ToA AoA	It can be integrated in applications and smartphones.	Requires microphone arrays and loudspeakers.

TABLE 5. (Continued.) Summary of different technologies for indoor localization.

Infrared	Few meters	Room-level	dm	Low	ToA TDoA	Orientation of cameras in talk assistance applications.	Interference from fluorescent and sunlight, LOS.
Lidar	10 m	Very high	mm-cm	High	ToA AoA	Commercially available. No RF interference.	LOS, not wearable. Dependence on lightening conditions.
Visual	10 m	High	mm-cm	Medium	AoA TDoA RSSI	Commercially available. No RF interference.	Requires LOS. High computational requirements.
This work (Lora Backscatter)	<100 m	Very Low	Room level	Low	RSSI Fingerprint	Low number of anchors. Wearable. High immunity to inferences.	Requires a database for training the classifiers.

(CSI) [55] provided by some Wi-Fi boards. ToA has also been proposed, although it requires hardware modifications [56]. Angle-of-arrival (AoA) localization techniques were recently investigated in [57], [58]. Fingerprinting is a widely used indoor positioning method used with several wireless access technologies including Wi-Fi, BLE, and Zigbee [52]. This method can improve accuracy in NLOS environments, but it requires the creation of a database from training measurements and the results depend on the density of reference points.

**B. ZIGBEE**

Zigbee (IEEE 802.15.4 standard) based localization techniques [59], [60] share the primary drawback of Wi-Fi-based techniques. But the use of Zigbee networks (mainly used for wireless sensor networks) is not as widespread in indoor environments as Wi-Fi networks, and require an additional deployment that increases the cost of the localization system.

**C. UWB**

Ultra-wideband (UWB) is one of the wireless solutions that has been the focus of much attention for indoor localization. This interest arises from the fact that the use of large bandwidth yields high time resolution because it is possible to separate multiple reflections from the pulse. As a consequence, UWB systems can obtain centimeter-level ranging accuracy under LOS conditions, even in indoor environments with multipath interferences [61]. The position is often

determined by trilateration from the measured ToA from different anchors distributed in the coverage area. Localization accuracy depends on the number of anchors, their location and the LOS coverage. To address the problem of cost-effective UWB-based localization in complex indoor environments, hybrid trilateration and fingerprint algorithms have been developed [62]. The cost of the system depends on the number of anchors. UWB technology is not as extensive as other wireless technologies and the cost of UWB transceivers is still expensive compared with other wireless systems (e.g. Wi-Fi or Bluetooth).

**D. BLUETOOTH**

The latest version of Bluetooth (IEEE 802.15.1) is known as Bluetooth Low Energy (BLE), which achieves a coverage range of 10–20 meters indoors with better energy efficiency compared to previous versions. The RSSI measurement provided by BLE devices can be used for localization [63]. However, two BLE based protocols, iBeacons (by Apple Inc.) and Eddystone (by Google, Inc.), have been designed for context-aware proximity services. From the messages received from the beacon and from the RSSI, users are classified into three range regions (immediate, near, far, or unknown) [64]. Based on the user’s proximity to any beacon, the mobile application triggers an action (e.g. sends a notification or a discount coupon) [65]. Fingerprint approaches based on iBeacon have been proposed in the literature [66], [67].

### E. RFID

RFID systems can be classified into active and passive. Active RFID is often used to track assets outdoors, where great position accuracy (order of meters) is not required and when measurements are taken over long periods of time that require long-lasting batteries. They are based on UHF (ISM 433 or 868 MHz bands) and ISM 2.45 GHz. Essentially, two different types of active RFID tags are available: transponders and beacons. With transponders, communication works by means of backscattering, but using battery-assisted (BAP) devices. Active RFID transponders are commonly used in secure access control and payment systems at toll booths. Battery-assisted UHF tags that comply with Gen 2 standards [68] (and therefore, can be read with standard UHF readers) have recently been released which can extend the range of passive RFID systems up to 20 m. In these BAP tags, the uplink read range is limited by the sensitivity of the reader as in passive UHF tags. However, some active RFID tags use beacon tags. These tags use a transmitter that sends out messages every few seconds. The use of transmitters extends the read range but can noticeably reduce the battery life depending on the transmission duty-cycle used. Active tag beacons are very common in the oil and gas industry, and for cargo tracking systems. For example, commercial Tagsense tags use a modified Zigbee transmitter, and Omni-ID integrates BLE and LoRaWAN transceivers. The read range in the open field is about 80 m depending on the antennas used [69]. This read range is notably reduced in indoor environments to 20 m [70] due to multipath propagation. The sensitivity of a typical reader is on the order of  $-100$  dBm. The price of active RFID tags is between \$20 and \$100 depending on their functionality and whether they must withstand harsh conditions. Although active RFID is designed for outdoor applications, it has been explored for indoor localization applications as well. LANDMARC is one of the most popular indoor localization technologies used in active RFID tags [71]–[73].

Passive tags, on the other hand, have shorter transmission ranges because they do not use a battery. They therefore have a lower read range than active RFID tags. UHF RFID can read up to a few meters, but HF RFID and NFC can read up to a few centimeters. Although they have the advantage of low cost, UHF readers are more expensive than the NFC readers available in modern smartphones. A navigation system based on NFC has recently been proposed in [74]. The limitations on coverage make passive RFID suitable for proximity applications [75].

### F. ACOUSTIC

Radiofrequency (RF) signals share many characteristics with acoustic signals. Compared to more common RF signals like Wi-Fi, acoustic localization has been gaining strength because its main requirements are microphones and speakers, which are widely equipped on many smart devices [76], [77].

Another advantage of the acoustic signal is that the speed of sound is much lower than the speed of a RF signal, which is a positive factor in achieving higher accuracy. Different localization techniques are being used that combine multiple microphone signals, such as those based on time of arrival (ToA), time difference of arrival (TDoA), Doppler effect, direction of arrival (DOA), and steered response power (SRP) [53]. One advantage of these devices is that they can use the microphones built into smartphones [78].

### G. ULTRASOUND

Ultrasound-based localization technology uses ultrasound waves (typically at 44 kHz) to measure the ToA between a transmitter and a receiver [79], [80]. Due to the lower velocity of sound compared to that of an electromagnetic wave, accuracies of less than centimeters can be achieved in range measurements. For node synchronization, the ultrasound localization system requires a secondary RF link. One disadvantage of these systems is the dependence of sound velocity on temperature and humidity and the high levels of environmental noise, which reduce accuracy and coverage.

### H. VISUAL SYSTEMS

Visual localization systems are commercially available on the market (e.g. Kinect [81] or Wii [82] for games). They do not have interferences from RF devices, but they are affected by environmental lighting conditions and pose privacy issues. Another disadvantage of this technology is the high computational requirements that make it difficult to integrate into smartphones or wearables. These systems also require LOS, limiting their coverage to only a few meters [83].

### I. VISIBLE LIGHT

Visible light-based localization techniques use light sensors to measure the position and direction of LED emitters that work something like iBeacons. The localization is based on AoA methods [84]. The advantage of this technology is its low cost, which makes it possible to install the LEDs over large areas. However, the biggest drawback with this technology, as with other techniques based on light, is the need for LOS.

### J. LIDAR

LIDARs and infrared cameras are becoming more popular in robotics [85] as their accuracy is in the order of millimeters. LIDAR is fast and accurate and it is gaining popularity with car makers due its use in the development of autonomous cars [86]. Although LIDAR systems are becoming increasingly common, such systems are still expensive.

### K. INFRARED (IR)

The low cost of IR positioning systems makes them a potential candidate at the room level, though their coverage range and accuracy are limited [87]. Technical limitations

such as the required LOS between the transmitter and the receiver and the interference of IR waves with fluorescent light and sunlight reduce the widespread usability of these systems. These issues have led researchers to explore alternative approaches to infrared-based indoor positioning.

### L. PROPOSED SOLUTION BASED ON LoRa BACKSCATTER

The main novelty of the proposed system is the utilization of a LoRa backscatter. With the exception of RFID systems, which also rely on backscattering communication, other wireless systems use communication between a transmitter and receiver. Consequently, the power consumption of the proposed system is lower than even BLE and Zigbee devices. We have presented a low-cost (< \$5) proof-of-concept of a wearable device. The prototype can run continuously for 24 days or for more than two years if the refresh rate is reduced to 1/10 seconds with a 500 mAh Lite-on battery. The proposed system has been designed for room-level localization; however, other techniques based on RSSI, such as Wi-Fi, Zigbee or BLE can also be applied. The computational cost of the algorithm is low, and it is implemented on a server. Low power consumption is a key advantage as it eliminates the need for frequent battery replacement, which can be an issue in ADL applications for use with the elderly. This long battery life also means that the system can be used to track assets in indoor environments. The high sensitivity of LoRa receivers and their great immunity to interferences [88] due to the robustness of the CSS-modulation scheme allow a higher coverage range than other backscatters, including active RFID based on proprietary protocols. The use of lower frequencies reduces the undesirable effects associated with the attenuation and diffraction by the body compared with systems operating in 2.45 GHz bands. In addition, in some countries, the ISM 433 MHz band can be used for LoRa (e.g. based on Semtech SX1278 [19]) allowing the coverage range to be expanded. The result is better for indoor coverage, reducing the number of anchors or reference nodes and improving performance in wearable applications. LoRa is also a low-cost, low-power standardized wireless system that is continuously growing. Therefore, the cost of LoRa transceivers is lower than active UHF RFID readers. Low-cost Wi-Fi nodes with LoRa transceivers are used as receivers, therefore the use of expensive multichannel gateways or routers is not required. For example, in this work, a low-cost ESP32 shield with a Semtech SX1276 transceiver was used in the experiments. Therefore, the overall cost of the system is lower than UWB and comparable to Wi-Fi or Zigbee based systems.

Device-free localization (DFL) techniques have been proposed using the variation of the RSSI received from different signals in a wireless network to detect and count the presence of human activity [89]. Although DFL has several interesting applications, the results are likely to be more sensitive to environmental changes. Fingerprint-based algorithms are

often used in DFL. However, the training data requires several measurements with a person standing at different positions to avoid the influence of measurement noise. Also, training environments with multiple people who backscatter the signals is challenging [89]. In the proposed system, the multiple signals backscattered on different objects in the scene are filtered from those produced by the LoRa backscatter because they change the frequency to another channel.

### VI. CONCLUSION

Techniques for estimating the absolute positions of users in a coordinate system have been widely researched. Today, applications can locate a person or an object within a building by merely monitoring the room in which that individual or item is located. This paper presents an indoor localization system with room-level accuracy and a focus on easy setup and a low-cost network. The system is based on the analysis of the backscattered signal strength received by LoRa transceivers deployed in an indoor environment. The backscatter device stands out for its low power consumption and long range. This paper has explored different methods, ranging from a simple technique that assigns the room to the receiver with the highest measurement value to other more sophisticated techniques based on machine learning. The method based on the highest level detected exhibits great accuracy as long as the coverage is good in all rooms. Otherwise, to obtain better accuracy, methods based on machine learning are required. In these cases, a process to train the classification algorithms is necessary. This is a quick and straightforward process that only requires taking random samples in each room, without the need to determine the absolute coordinates at the sampling points. The proposed method also does not require establishing a propagation model, unlike other existing methods in the literature. The use of a low-cost, low-consumption LoRa backscatter device eliminates the need for frequent battery recharging, unlike in devices with higher consumption. Our experimental results show that the LoRa backscatter can be detected through the walls in indoor environments. The LoRa backscatter can be easily integrated into a comfortable wrist band. Due to the high sensitivity of the LoRa system, a large number of anchors are not required. Simulated and experimental results show that only one receiver in each room and a transmitter for every three to four receivers are needed to locate a person at the floor level in a standard home. The wireless network required can be implemented using low-cost modules available on the market without any modification. The backend system can be implemented in any computer without the need for expensive servers using MQTT protocol.

### REFERENCES

- [1] J. Landt, "The history of RFID," *IEEE Potentials*, vol. 24, no. 4, pp. 8–11, Oct. 2005.
- [2] K. Finkenzeller, *RFID Handbook: Fundamentals and Applications in Contactless Smart Cards, Radio Frequency Identification and Near-Field Communication*. Hoboken, NJ, USA: Wiley, 2014.

- [3] W. Liu, K. Huang, X. Zhou, and S. Durrani, "Next generation backscatter communication: Systems, techniques, and applications," *EURASIP J. Wireless Commun. Netw.*, vol. 2019, no. 1, pp. 1–11, Dec. 2019.
- [4] N. Van Huynh, D. T. Hoang, X. Lu, D. Niyato, P. Wang, and D. I. Kim, "Ambient backscatter communications: A contemporary survey," *IEEE Commun. Surveys Tuts.*, vol. 20, no. 4, pp. 2889–2922, 4th Quart., 2018.
- [5] P. Zhang, M. Rostami, P. Hu, and D. Ganesan, "Enabling practical backscatter communication for on-body sensors," in *Proc. ACM SIGCOMM Conf.*, Aug. 2016, pp. 370–383.
- [6] S. J. Thomas, J. S. Besnoff, and M. S. Reynolds, "Modulated backscatter for ultra-low power uplinks from wearable and implantable devices," in *Proc. ACM Workshop Med. Commun. Syst. (MedCOMM)*, 2012, pp. 1–6.
- [7] S. N. Daskalakis, A. Georgiadis, G. Goussetis, and M. M. Tentzeris, "Low cost ambient backscatter for agricultural applications," in *Proc. IEEE-APS Topical Conf. Antennas Propag. Wireless Commun. (APWC)*, Sep. 2019, p. 201.
- [8] F. Adelantado, X. Vilajosana, P. Tuset-Peiro, B. Martinez, J. Melia-Segui, and T. Watteyne, "Understanding the limits of LoRaWAN," *IEEE Commun. Mag.*, vol. 55, no. 9, pp. 34–40, Sep. 2017.
- [9] J. C. de Silva, J. J. P. C. Rodrigues, A. M. Alberti, P. Solic, and A. L. L. Aquino, "LoRaWAN—A low power WAN protocol for Internet of Things: A review and opportunities," in *Proc. 2nd Int. Multidisciplinary Conf. Comput. Energy Sci. (SplitTech)*, Jul. 2017, pp. 1–6.
- [10] D. Bankov, E. Khorov, and A. Lyakhov, "On the limits of LoRaWAN channel access," in *Proc. Int. Conf. Eng. Telecommun. (EnT)*, Nov. 2016, pp. 10–14.
- [11] L. Vangelista, "Frequency shift chirp modulation: The LoRa modulation," *IEEE Signal Process. Lett.*, vol. 24, no. 12, pp. 1818–1821, Dec. 2017.
- [12] Semtech. 2019. *SX1276/77/78/79–137 MHz to 1020 MHz Low Power Long Range Transceiver*. Accessed: Feb. 14, 2020. [Online]. Available: [https://semtech.my.salesforce.com/sfc/p/E0000000JelG/a/2R0000001OKs/Bs97dmPXeatnbdoJNVMIaKDIQz8q1N\\_gx8Dcgqi7g2o](https://semtech.my.salesforce.com/sfc/p/E0000000JelG/a/2R0000001OKs/Bs97dmPXeatnbdoJNVMIaKDIQz8q1N_gx8Dcgqi7g2o)
- [13] T. Ameloot, P. Van Torre, and H. Rogier, "LoRa indoor performance: An office environment case study," in *Proc. Int. Appl. Comput. Electromagn. Soc. Symp.-China (ACES)*, Jul. 2018, pp. 1–2.
- [14] J. Petäjäjärvi, K. Mikhaylov, R. Yasmin, M. Hämäläinen, and J. Iinatti, "Evaluation of LoRa LPWAN technology for indoor remote health and wellbeing monitoring," *Int. J. Wireless Inf. Netw.*, vol. 24, no. 2, pp. 153–165, Jun. 2017.
- [15] J. Zhao, W. Gong, and J. Liu, "X-tandem: Towards multi-hop backscatter communication with commodity WiFi," in *Proc. 24th Annu. Int. Conf. Mobile Comput. Netw.*, 2018, pp. 497–511.
- [16] A. Varshney, O. Harms, C. Pérez-Penichet, C. Rohner, F. Hermans, and T. Voigt, "LoRea: A backscatter architecture that achieves a long communication range," in *Proc. 15th ACM Conf. Embedded Netw. Sensor Syst.*, 2017, pp. 1–14.
- [17] Y. Peng, L. Shangquan, Y. Hu, Y. Qian, and X. Lin, "PLoRa: A passive long-range data network from ambient LoRa transmissions," in *Proc. Conf. ACM Special Interest Group Data Commun.*, 2018, pp. 147–160.
- [18] V. Talla, M. Hesar, B. Kellogg, A. Najafi, J. R. Smith, and S. Gollakota, "LoRa backscatter: Enabling the vision of ubiquitous connectivity," *Proc. ACM Interact., Mobile, Wearable Ubiquitous Technol.*, vol. 1, no. 3, pp. 1–24, 2017.
- [19] M. Lazaro, A. Lazaro, and R. Villarino, "Feasibility of backscatter communication using LoRAWAN signals for deep implanted devices and wearable applications," *Sensors*, vol. 20, no. 21, p. 6342, Nov. 2020.
- [20] F. Zafari, A. Gkelias, and K. K. Leung, "A survey of indoor localization systems and technologies," *IEEE Commun. Surveys Tuts.*, vol. 21, no. 3, pp. 2568–2599, 3rd Quart., 2019.
- [21] A. Yassin, Y. Nasser, M. Awad, A. Al-Dubai, R. Liu, C. Yuen, R. Raulefs, and E. Aboutanos, "Recent advances in indoor localization: A survey on theoretical approaches and applications," *IEEE Commun. Surveys Tuts.*, vol. 19, no. 2, pp. 1327–1346, 2nd Quart., 2017.
- [22] J. Xiao, Z. Zhou, Y. Yi, and L. M. Ni, "A survey on wireless indoor localization from the device perspective," *ACM Comput. Surv.*, vol. 49, no. 2, pp. 1–31, Nov. 2016.
- [23] F. Seco, A. R. Jimenez, C. Prieto, J. Roa, and K. Koutsou, "A survey of mathematical methods for indoor localization," in *Proc. IEEE Int. Symp. Intell. Signal Process.*, Aug. 2009, pp. 9–14.
- [24] A. N. Raghavan, H. Ananthapadmanaban, M. S. Sivamurugan, and B. Ravindran, "Accurate mobile robot localization in indoor environments using bluetooth," in *Proc. IEEE Int. Conf. Robot. Autom.*, May 2010, pp. 4391–4396.
- [25] K.-H. Lam, C.-C. Cheung, and W.-C. Lee, "RSSI-based LoRa localization systems for large-scale indoor and outdoor environments," *IEEE Trans. Veh. Technol.*, vol. 68, no. 12, pp. 11778–11791, Dec. 2019.
- [26] K.-H. Lam, C.-C. Cheung, and W.-C. Lee, "New RSSI-based LoRa localization algorithms for very noisy outdoor environment," in *Proc. IEEE 42nd Annu. Comput. Softw. Appl. Conf. (COMPSAC)*, vol. 2, Jul. 2018, pp. 794–799.
- [27] Y.-C. Lin, C.-C. Sun, and K.-T. Huang, "RSSI measurement with channel model estimating for IoT wide range localization using LoRa communication," in *Proc. Int. Symp. Intell. Signal Process. Commun. Syst. (ISPACS)*, Dec. 2019, pp. 1–2.
- [28] Y. Li, Z. He, Y. Li, H. Xu, L. Pei, and Y. Zhang, "Towards location enhanced IoT: Characterization of LoRa signal for wide area localization," in *Proc. Ubiquitous Positioning, Indoor Navigat. Location-Based Services (UPINLBS)*, Mar. 2018, pp. 1–7.
- [29] P. Moravek, D. Komosny, M. Simek, M. Jelinek, D. Girbau, and A. Lazaro, "Investigation of radio channel uncertainty in distance estimation in wireless sensor networks," *Telecommun. Syst.*, vol. 52, no. 3, pp. 1549–1558, Mar. 2013.
- [30] P. Moravek, D. Komosny, M. Simek, D. Girbau, and A. Lazaro, "Energy analysis of received signal strength localization in wireless sensor networks," *Radioengineering*, vol. 20, no. 4, pp. 937–945, 2011.
- [31] D. Cabarkapa, I. Grujic, and P. Pavlovic, "Comparative analysis of the Bluetooth low-energy indoor positioning systems," in *Proc. 12th Int. Conf. Telecommun. Modern Satell., Cable Broadcast. Services (TELSIKS)*, Oct. 2015, pp. 76–79.
- [32] Z. Yang, C. Wu, and Y. Liu, "Locating in fingerprint space: Wireless indoor localization with little human intervention," in *Proc. 18th Annu. Int. Conf. Mobile Comput. Netw.*, 2012, pp. 269–280.
- [33] M. Li, L. Zhao, D. Tan, and X. Tong, "BLE fingerprint indoor localization algorithm based on eight-neighborhood template matching," *Sensors*, vol. 19, no. 22, p. 4859, Nov. 2019.
- [34] T. Tegou, I. Kalamaras, K. Votis, and D. Tzovaras, "A low-cost room-level indoor localization system with easy setup for medical applications," in *Proc. 11th IFIP Wireless Mobile Netw. Conf. (WMNC)*, Sep. 2018, pp. 1–7.
- [35] G. Y. Ha, S. B. Seo, H. S. Oh, and W. S. Jeon, "LoRa ToA-based localization using fingerprint method," in *Proc. Int. Conf. Inf. Commun. Technol. Converg. (ICTC)*, Oct. 2019, pp. 349–353.
- [36] M. Aermouts, R. Berkvens, K. Van Vlaenderen, and M. Weyn, "Sigfox and LoRaWAN datasets for fingerprint localization in large urban and rural areas," *Data*, vol. 3, no. 2, p. 13, Apr. 2018.
- [37] Y. Basiouny, M. Arafa, and A. M. Sarhan, "Enhancing Wi-Fi fingerprinting for indoor positioning system using single multiplicative neuron and PCA algorithm," in *Proc. 12th Int. Conf. Comput. Eng. Syst. (ICCES)*, Dec. 2017, pp. 295–305.
- [38] L. Gogolak, S. Pletl, and D. Kukulj, "Indoor fingerprint localization in WSN environment based on neural network," in *Proc. IEEE 9th Int. Symp. Intell. Syst. Informat.*, Sep. 2011, pp. 293–296.
- [39] L. B. Del Mundo, R. L. D. Ansay, C. A. M. Festin, and R. M. Ocampo, "A comparison of wireless fidelity (Wi-Fi) fingerprinting techniques," in *Proc. ICTC*, Sep. 2011, pp. 20–25.
- [40] R. Jia, M. Jin, Z. Chen, and C. J. Spanos, "SoundLoc: Accurate room-level indoor localization using acoustic signatures," in *Proc. IEEE Int. Conf. Autom. Sci. Eng. (CASE)*, Aug. 2015, pp. 186–193.
- [41] P. Martin, B.-J. Ho, N. Grupen, S. Muñoz, and M. Srivastava, "An iBeacon primer for indoor localization: Demo abstract," in *Proc. 1st ACM Conf. Embedded Syst. Energy-Efficient Buildings*, 2014, pp. 190–191.
- [42] C. Debes, A. Merentitis, S. Sukhanov, M. Niessen, N. Frangiadakis, and A. Bauer, "Monitoring activities of daily living in smart homes: Understanding human behavior," *IEEE Signal Process. Mag.*, vol. 33, no. 2, pp. 81–94, Mar. 2016.
- [43] S. Blackman, C. Matlo, C. Bobrovitskiy, A. Waldoch, M. L. Fang, P. Jackson, A. Mihailidis, L. Nygård, A. Astell, and A. Sixsmith, "Ambient assisted living technologies for aging well: A scoping review," *J. Intell. Syst.*, vol. 25, no. 1, pp. 55–69, Jan. 2016.

- [44] M. Johannes Tiusanen, "Soil scouts: Description and performance of single hop wireless underground sensor nodes," *Ad Hoc Netw.*, vol. 11, no. 5, pp. 1610–1618, Jul. 2013.
- [45] I. Susnea, L. Dumitriu, M. Talmaciu, E. Pecheanu, and D. Munteanu, "Unobtrusive monitoring the daily activity routine of elderly people living alone, with low-cost binary sensors," *Sensors*, vol. 19, no. 10, p. 2264, May 2019.
- [46] A. Lazaro, J. Lorenzo, R. Villarino, and D. Girbau, "Backscatter transponder based on frequency selective surface for FMCW radar applications," *Radioengineering*, vol. 23, no. 2, pp. 632–641, 2014.
- [47] P. V. Nikitin, K. V. S. Rao, and R. D. Martinez, "Differential RCS of RFID tag," *Electron. Lett.*, vol. 43, no. 8, pp. 431–432, Apr. 2007.
- [48] D. Pena, R. Feick, H. D. Hristov, and W. Grote, "Measurement and modeling of propagation losses in brick and concrete walls for the 900-MHz band," *IEEE Trans. Antennas Propag.*, vol. 51, no. 1, pp. 31–39, Jan. 2003.
- [49] A. Lazaro, D. Girbau, and D. Salinas, "Radio link budgets for UHF RFID on multipath environments," *IEEE Trans. Antennas Propag.*, vol. 57, no. 4, pp. 1241–1251, Apr. 2009.
- [50] A. Goldsmith, *Wireless Communication*. Cambridge, U.K.: Cambridge Univ. Press, 2005.
- [51] F. Pedregosa, G. Varoquaux, and A. Gramfort, "Scikit-learn: Machine learning in Python," *J. Mach. Learn. Res.*, vol. 12, pp. 2825–2830, Oct. 2011.
- [52] A. Nessa, B. Adhikari, F. Hussain, and X. N. Fernando, "A survey of machine learning for indoor positioning," *IEEE Access*, vol. 8, pp. 214945–214965, 2020.
- [53] S. Xie, Y. Hu, and Y. Wang, "Weighted centroid localization algorithm based on least square for wireless sensor networks," in *Proc. IEEE Int. Conf. Consum. Electron.-China*, Apr. 2014, pp. 1–4.
- [54] B. Yang, L. Guo, R. Guo, M. Zhao, and T. Zhao, "A novel trilateration algorithm for RSSI-based indoor localization," *IEEE Sensors J.*, vol. 20, no. 14, pp. 8164–8172, Jul. 2020.
- [55] L. Zhao, H. Wang, P. Li, and J. Liu, "An improved WiFi indoor localization method combining channel state information and received signal strength," in *Proc. 36th Chin. Control Conf. (CCC)*, Jul. 2017, pp. 8964–8969.
- [56] M. Youssef, A. Youssef, C. Rieger, U. Shankar, and A. Agrawala, "Pin-Point: An asynchronous time-based location determination system," in *Proc. 4th Int. Conf. Mobile Syst., Appl. Services*, 2006, pp. 165–176.
- [57] L. N. Kandel and S. Yu, "VWAN: Virtual WiFi Antennas for increased indoor localization accuracy," in *Proc. IEEE Int. Conf. Ind. Internet (ICII)*, Nov. 2019, pp. 258–267.
- [58] Z. Tian, Z. Wang, Z. Li, and M. Zhou, "RTIL: A real-time indoor localization system by using angle of arrival of commodity WiFi signal," in *Proc. 11th Int. Conf. Wireless Commun. Signal Process. (WCSP)*, Oct. 2019, pp. 1–6.
- [59] J. Blumenthal, R. Grossmann, F. Golasowski, and D. Timmermann, "Weighted centroid localization in zigbee-based sensor networks," in *Proc. IEEE Int. Symp. Intell. Signal Process.*, Oct. 2007, pp. 1–6.
- [60] H. P. Pradityo, L. Rosyidi, Misbahuddin, and R. F. Sari, "Performance evaluation of RSS fingerprinting method to track ZigBee devices location using artificial neural networks," in *Proc. Int. Conf. Inf. Commun. Technol. Converg. (ICTC)*, Oct. 2017, pp. 268–273.
- [61] D. Dardari, A. Conti, U. Ferner, A. Giorgetti, and M. Z. Win, "Ranging with ultrawide bandwidth signals in multipath environments," *Proc. IEEE*, vol. 97, no. 2, pp. 404–426, Feb. 2009.
- [62] S. Djovic, I. Stojanovic, M. Jovanovic, T. Nikolic, and G. L. Djordjevic, "Fingerprinting-assisted UWB-based localization technique for complex indoor environments," *Expert Syst. Appl.*, Nov. 2020, Art. no. 114188.
- [63] R. Faragher and R. Harle, "Location fingerprinting with Bluetooth low energy beacons," *IEEE J. Sel. Areas Commun.*, vol. 33, no. 11, pp. 2418–2428, Nov. 2015.
- [64] V. Andruschchak, T. Maksymyuk, M. Klymash, and D. Ageyev, "Development of the iBeacon's positioning algorithm for indoor scenarios," in *Proc. Int. Sci.-Practical Conf. Problems Infocommun. Sci. Technol. (PIC S&T)*, Oct. 2018, pp. 741–744.
- [65] Z. He, B. Cui, W. Zhou, and S. Yokoi, "A proposal of interaction system between visitor and collection in museum Hall by iBeacon," in *Proc. 10th Int. Conf. Comput. Sci. Edu. (ICCSE)*, Jul. 2015, pp. 427–430.
- [66] J. Zuo, S. Liu, H. Xia, and Y. Qiao, "Multi-phase fingerprint map based on interpolation for indoor localization using iBeacons," *IEEE Sensors J.*, vol. 18, no. 8, pp. 3351–3359, Apr. 2018.
- [67] T.-M.-T. Dinh, N.-S. Duong, and K. Sandrasegaran, "Smartphone-based indoor positioning using BLE iBeacon and reliable lightweight fingerprint map," *IEEE Sensors J.*, vol. 20, no. 17, pp. 10283–10294, Sep. 2020.
- [68] J. Jung, H. Kim, H. Lee, and K. Yeom, "An UHF RFID tag with long read range," in *Proc. Eur. Microw. erence (EuMC)*, 2009, pp. 1113–1116.
- [69] M. Cassel, T. Dépret, and H. Piégay, "Assessment of a new solution for tracking pebbles in rivers based on active RFID," *Earth Surf. Processes Landforms*, vol. 42, no. 13, pp. 1938–1951, Oct. 2017.
- [70] S. Xu, H. Zhou, C. Wu, C.-M. Huang, and S. Moon, "Spatial signal attenuation model of active RFID tags," *IEEE Access*, vol. 6, pp. 6947–6960, 2018.
- [71] L. M. Ni, Y. Liu, Y. Cho Lau, and A. P. Patil, "LANDMARC: Indoor location sensing using active RFID," in *Proc. 1st IEEE Int. Conf. Pervas. Comput. Commun. (PerCom)*, Mar. 2003, pp. 407–415.
- [72] G.-y. Jin, X.-y. Lu, and M.-S. Park, "An indoor localization mechanism using active RFID tag," in *Proc. IEEE Int. Conf. Sensor Netw., Ubiquitous, Trustworthy Comput. (SUTC)*, vol. 1, Jun. 2006, p. 4.
- [73] J. Wang, R. K. Dhanapal, P. Ramakrishnan, B. Balasingam, T. Souza, and R. Maev, "Active RFID based indoor localization," in *Proc. 22th Int. Conf. Inf. Fusion (FUSION)*, Jul. 2019, pp. 1–7.
- [74] W. E. Sakkpere, N. B. W. Mlitwa, and M. A. Oshin, "Towards an efficient indoor navigation system: A near field communication approach," *J. Eng., Des. Technol.*, vol. 15, no. 4, pp. 505–527, Aug. 2017.
- [75] S. Siachalou, S. Megalou, A. Tzitzis, E. Tsardoulis, A. Bletsas, J. Sahalos, T. Yioultis, and A. G. Dimitriou, "Robotic inventorying and localization of RFID tags, exploiting phase-fingerprinting," in *Proc. IEEE Int. Conf. RFID Technol. Appl. (RFID-TA)*, Sep. 2019, pp. 362–367.
- [76] M. Cobos, F. Antonacci, A. Alexandridis, A. Mouchtaris, and B. Lee, "A survey of sound source localization methods in wireless acoustic sensor networks," *Wireless Commun. Mobile Comput.*, vol. 2017, Aug. 2017, Art. no. 3956282.
- [77] M. Liu, L. Cheng, K. Qian, J. Wang, J. Wang, and Y. Liu, "Indoor acoustic localization: A survey," *Hum.-Centric Comput. Inf. Sci.*, vol. 10, no. 1, p. 2, Dec. 2020.
- [78] H. Chen, F. Li, and Y. Wang, "EchoLoc: Accurate device-free hand localization using COTS devices," in *Proc. 45th Int. Conf. Parallel Process. (ICPP)*, Aug. 2016, pp. 334–339.
- [79] F. Ijaz, H. K. Yang, A. W. Ahmad, and C. Lee, "Indoor positioning: A review of indoor ultrasonic positioning systems," in *Proc. 15th Int. Conf. Adv. Commun. Technol. (ICACT)*, Jan. 2013, pp. 1146–1150.
- [80] C. Medina, J. Segura, and Á. De la Torre, "Ultrasound indoor positioning system based on a low-power wireless sensor network providing sub-centimeter accuracy," *Sensors*, vol. 13, no. 3, pp. 3501–3526, Mar. 2013.
- [81] J. Shotton, A. Fitzgibbon, M. Cook, T. Sharp, M. Finocchio, R. Moore, A. Kipman, and A. Blake, "Real-time human pose recognition in parts from single depth images," in *Proc. CVPR*, Jun. 2011, pp. 1297–1304.
- [82] T. Schlömer, B. Poppinga, N. Henze, and S. Boll, "Gesture recognition with a wii controller," in *Proc. 2nd Int. Conf. Tangible Embedded Interact. (TEI)*, 2008, pp. 11–14.
- [83] F. Alkhwaja, M. Jaradat, and L. Romdhane, "Techniques of indoor positioning systems (IPS): A survey," in *Proc. Adv. Sci. Eng. Technol. Int. Conf. (ASET)*, Mar. 2019, pp. 1–8.
- [84] Y.-S. Kuo, P. Pannuto, K.-J. Hsiao, and P. Dutta, "Luxapose: Indoor positioning with mobile phones and visible light," in *Proc. 20th Annu. Int. Conf. Mobile Comput. Netw.*, 2014, pp. 447–458.
- [85] Y. Xu, Y. S. Shmaliy, Y. Li, X. Chen, and H. Guo, "Indoor INS/LiDAR-based robot localization with improved robustness using cascaded FIR filter," *IEEE Access*, vol. 7, pp. 34189–34197, 2019.
- [86] R. W. Wolcott and R. M. Eustice, "Visual localization within LIDAR maps for automated urban driving," in *Proc. IEEE/RSJ Int. Conf. Intell. Robots Syst.*, Sep. 2014, pp. 176–183.
- [87] E. Aitenbichler and M. Muhlhauser, "An IR local positioning system for smart items and devices," in *Proc. 23rd Int. Conf. Distrib. Comput. Syst. Workshops*, 2003, pp. 334–339.
- [88] T. Elshabrawy and J. Robert, "The impact of ISM interference on LoRa BER performance," in *Proc. IEEE Global Conf. Internet Things (GCIoT)*, Dec. 2018, pp. 1–5.
- [89] N. Patwari and J. Wilson, "RF sensor networks for device-free localization: Measurements, models, and algorithms," *Proc. IEEE*, vol. 98, no. 11, pp. 1961–1973, Nov. 2010.



**ANTONIO LAZARO** (Senior Member, IEEE) was born in Lleida, Spain, in 1971. He received the M.S. and Ph.D. degrees in telecommunication engineering from the Universitat Politècnica de Catalunya (UPC), Barcelona, Spain, in 1994 and 1998, respectively. He then joined the faculty of the UPC, where he currently teaches a course on microwave circuits and antennas. Since July 2004, he has been a full-time Professor with the Department of Electronic Engineering, Universitat Rovira i Virgili (URV), Tarragona, Spain. His research interests include microwave device modeling, on-wafer noise measurements, monolithic microwave integrated circuits (MMICs), low-phase noise oscillators, MEMS, RFID, UWB, and microwave systems.



**MARC LAZARO** was born in Tarragona, Spain, in 1995. He received the B.S. degree in industrial electronics and automation engineering and the M.S. degree in electronic systems engineering and technology (METSE) from Rovira i Virgili University, Tarragona, Spain, in 2017 and 2018, respectively, where he is currently pursuing the Ph.D. degree with the Department of Electronics. Up until now, he has been accumulated professional experience as a Data Acquisition Engineer and as an Embedded Systems Developer. His research interests include semipassive RFID technologies based on backscattering communication and novel applications based on millimeter wave identification (MMID).



**RAMON VILLARINO** received the degree in telecommunications technical engineering from Ramon Llull University (URL), Barcelona, Spain, in 1994, the degree in senior telecommunications engineering and the Ph.D. degree from the Universitat Politècnica de Catalunya (UPC), Barcelona, in 2000 and 2004, respectively. From 2005 to 2006, he was a Research Associate with the Technological Telecommunications Center of Catalonia (CTTC), Barcelona. He worked as a Researcher and an Assistant Professor with the Universitat Autònoma de Barcelona (UAB), from 2006 to 2008. Since January 2009, he has been a full-time Professor with Universitat Rovira i Virgili (URV), Tarragona, Spain. His research interests include radiometry, microwave devices, and systems based on UWB, RFIDs, and frequency selective structures using metamaterials (MM).

...